IEEE Access
Multidisciplinary : Rapid Review : Open Access Journal

Received November 11, 2021, accepted December 2, 2021, date of publication December 6, 2021, date of current version December 17, 2021.

Digital Object Identifier 10.1109/ACCESS.2021.3133023

A Modulated Model-Free Predictive Current Control for Four-Switch Three-Phase Inverter-Fed SynRM Drive Systems

CHENG-KAI LIN[1], CRESTIAN ALMAZAN AGUSTIN[1], (Graduate Student Member, IEEE), JEN-TE YU[2], YU-SHAN CHENG[1], (Member, IEEE), FU-MIN CHEN[1], AND YEN-SHIN LAI[3], (Fellow, IEEE)

[1]Department of Electrical Engineering, National Taiwan Ocean University, Keelung 202301, Taiwan
[2]Department of Electrical Engineering, Chung Yuan Christian University, Taoyuan City 320314, Taiwan
[3]Department of Electrical Engineering, National Taipei University of Technology, Taipei 106344, Taiwan

Corresponding author: Cheng-Kai Lin (cklin@mail.ntou.edu.tw)

This work was supported by the Ministry of Science and Technology, Taiwan, under Grant MOST-109-2221-E-019-022-MY2.

ABSTRACT This paper presents a modulated model-free predictive current control for four-switch three-phase inverter-fed synchronous reluctance motor drive systems to improve performance against existing methods. The study focuses on six switching modes modulated with variable duty ratios that are optimized and computed in real-time. The stator currents corresponding to the six modulated switching modes are predicted without relying on the motor's mathematical model nor parameters thanks to its model-free nature. To enhance the performance of the controller, adaptive current detection technique and current difference modification are employed, yielding good adaptation to the duty ratio modulations. Implementation of the proposed method is realized *via* a TMS320F28379D microcontroller on a testbed to assess its effectiveness. Finally, comparisons between the proposed scheme and a non-adaptive predecessor under various experimental settings are made to demonstrate its salient performance.

INDEX TERMS Four-switch three-phase inverter, modulated model-free predictive current control, synchronous reluctance motor, modulation.

I. INTRODUCTION

Motor drives have been widely explored over the years due to their extraordinary performances in torque control and speed response [1]–[3]. Thanks to the advent of various power electronic components, many industrial applications have been dramatically improved the quality, performance, and stability, including traction motors, variable frequency drives, and emerging technologies in the field of renewable energy [4]. Despite the apparent progress and developments in the field, sustainable and efficient control schemes remain a significant challenge [5].

Traditionally, the six-switch three-phase (SSTP) inverters are employed in most of these applications. Huber *et al.* [6] presented a multi-level inverter based on the SSTP topology that exhibits effective DC-link voltage regulations. Although the implementation is straightforward due to the absence of the neutral-point connection, such inverter topology has a subtle response to switching failures caused by an overload drive. The breakdown of the power switches is relevant to a transistor failure in the voltage source inverter (VSI) that leads to an open-circuit connection [7]. The power switch failure in the SSTP inverter has led to the development of an alternative reduced switching topology – the four-switch three-phase (FSTP) inverters [8]. Its unique feature benefits from fewer switching modes, cost-effectiveness, and simple logic signal generation [9], [10].

For synchronous reluctance motor (SynRM), various methods have been proposed to improve its performance, such as modern rotor geometries and effective control technologies. The unique rotor characteristics of the machine with no windings and embedded permanent magnets make it even more efficient and sustainable than other motor drives [11]. In fact, the SynRM has been touted as the future of AC machines because of its simple structure, robustness, high efficiency, and availability [12]. However, due to the highly

The associate editor coordinating the review of this manuscript and approving it for publication was Zhilei Yao.

nonlinear behavior exhibited by its components, an efficient and control system is still a significant challenge to date [13]. Some advances in nonlinear control have been reported as an alternative to the widely used PI-based field-oriented control (FOC), including the sliding mode control, fuzzy control [14], and artificial neural network-based control [15]. But the designs and implementations of these controllers are complicated. The model predictive current control (MPCC), on the other hand, holds some outstanding merits for its simplicity in accounting for nonlinearities and constraints [16]. It has been widely recognized as an excellent control scheme for motor drives and power inverters. However, there are still significant drawbacks that hamper the performance of MPCC, including the high degree of dependence on the accuracy of system parameters and the absence of a modulator [17]. The implementation of a single input voltage vector in each control period, in general, renders the reduction of current ripple and current error more difficult [18].

The modulation strategy based on duty cycle control [19], [20] and multiple vector applications [21], [22] was introduced to solve the problems encountered in the predictive controllers. Tarisciotti *et al.* [23] were the first to propose the modulated MPC (M2PC) to improve the current ripples of a seven-level H-bridge converter and a three-phase rectifier [17]. The method is anchored on the principle of space vector modulation, but it retains the salient features of multiobjective control and better performance against MPCC. In [24], the modulation is injected with a zero-sequence signal in optimizing the selection of switching states to improve the current harmonics and fast dynamic response of the controller but is delimited to passive load. A different modulation method based on deadbeat predictive control was proposed in [25], [26], where multiple cost functions are employed to identify the best composite voltage vector. In [18], [20], [27], multiple vectors are applied in each control cycle to reduce current ripples and errors. Although considerable improvements were obtained, as can be seen from the experimental results, these methods are model-based, relying mainly on the motor's precise mathematical model and system parameters. As a result, current predictions are sensitive to parameter mismatches and variations. Besides, the computational burden becomes a significant challenge due to overly complex algorithms that need to calculate individual duty cycles.

To circumvent the need for mathematical models and system parameters, Lin *et al.* [28], [29] proposed a model-free predictive current control (MFPCC) pioneering a current difference detection technique. In [30], the modulation combines two adjacent current vectors from a predefined first-level cost function. The over modulation region is controlled using a new rotating coordinate frame to keep the applied vector optimal. However, implementation in the modulation-based model-free control, particularly for FSTP inverters, remains less explored in the literature. In this paper, a novel modulation method, designated as modulated model-free predictive current control (MMFPCC) in the sequel, is presented to improve its predecessor [28], [29]. Compared to earlier methods, the main difference is that the proposed MMFPCC can predict the stator current under different voltage vectors at different application times. The presented method synthesizes two basic voltage vectors through a two-stage optimization process generating six switching modes with modulation advancing the limited numbers of candidate switching vectors of the FSTP inverter. Firstly, a performance index – a cost function – will be defined as a measure to represent the difference between the current command and the predicted current. Based on here, an optimal duty ratio is achieved *via* real-time calculation. Secondly, the optimal switching mode is obtained from candidates that minimize the cost function. Thanks to the high speed of the modern microcontroller, current differences corresponding to different application times can be measured and calculated in real-time. The proposed method is significantly different from [28] and [29], where the current difference calculation is done in a fixed application time manner. This variant of adaptive switching strategy makes it a technical breakthrough in the MFPCC.

The contributions of the proposed method are as follows:

1. The number of candidate voltage vectors for the FSTP inverter is boosted to six, known as switching modes. The vector synthesis is obtained from the linear modulation of two basic vectors, effectively reducing current ripples and errors.
2. The conduction durations of the two input voltage vectors are designed to be adaptive based on calculated optimal values. As such, the method employs an optimal scheme of two-vector-based switching to detect current sampling.
3. The updating scheme of stored current difference is performed twice in every sampling period based on modified current difference.
4. Optimization of duty cycles of the two input voltage vectors is obtained via minimizing a cost function.
5. Comprehensive experiments are conducted with promising results that support the proposed MMFPCC.

The rest of the article is organized as follows. The groundworks and the problems concerning MPCC and MFPCC are presented in Section II. Details of the proposed MMFPCC are given in Section III. Section IV presents the experimental results for the validation purpose of the proposed method. Finally, a conclusion is provided in Section V.

II. GROUNDWORKS AND EXISTING PROBLEMS

A. MPCC OF FSTP INVERTER-FED SYNRM

The generic topology of an FSTP inverter-fed SynRM is given in Fig. 1. As can be observed, the power switches in phase "c" are replaced by two capacitors, denoted as C_1 and C_2, respectively. The other two terminals have power switches, denoted as S_{a1}, S_{a0}, S_{b1}, and S_{b0}, respectively. Other fundamental variables include $\mathbf{i}_{a,b,c}$, $\mathbf{e}_{a,b,c}$, and $\mathbf{v}_{a,b,c}$ representing the phase-wise stator currents, the extended back-EMFs, and the stator voltages, respectively. L_q is the equivalent q-axis inductance, and r_s is the stator resistance.

As explained in [29], the simplified stator voltage equation of SynRM in the α-β reference coordinate can be written as

$$\mathbf{v}_x = r_s \mathbf{i}_x + L_q \frac{d\mathbf{i}_x}{dt} + \mathbf{e}_x, \quad x \in \{\alpha, \beta\}. \tag{1}$$

It is seen from (1) that different voltage vectors generated by the inverter will result in different stator currents. Given this condition, the FSTP inverter can only generate four switching states due to the absence of power switches in phase "c". The four basic voltage vectors are denoted by v_1, v_2, v_3, and v_4. This unique topology of the FSTP inverter reduces the number of power switches, hence hardware complexity and cost.

Based on the discretized counterpart of (1), the $(k+1)th$ stator current can be predicted as follows:

$$\mathbf{i}_x^p[k+1] = \frac{L_q - r_s T_s}{L_q}\mathbf{i}_x[k] + \frac{T_s}{L_q}\mathbf{v}_x[k] + \frac{1}{L_q}\mathbf{e}_x[k] \tag{2}$$

where superscript "p" denotes the predicted value, T_s is the sampling period, and $x \in \{\alpha, \beta\}$. It can be seen from (2) that the values of motor parameters, extended back-EMF, stator current, and stator voltage are all required in current prediction rendering a substantial disadvantage.

B. THE MFPCC

MFPCC scheme was first proposed by Lin *et al.* [28] based on a current difference detection technique. The implementation of the method is straightforward, as the current differences are directly calculated using the subtraction operations only. As illustrated in Fig. 2, there are two current differences, defined respectively as

$$\Delta\mathbf{i}_{\alpha,\beta}\Big|_{S^k}^{T_s} = \mathbf{i}_{\alpha,\beta}[k+1] - \mathbf{i}_{\alpha,\beta}[k] \tag{3}$$

$$\Delta\mathbf{i}_{\alpha,\beta}\Big|_{S^{k+1}}^{T_s} = \mathbf{i}_{\alpha,\beta}[k+2] - \mathbf{i}_{\alpha,\beta}[k+1]. \tag{4}$$

Given these equations, the current prediction can be expressed as

$$\mathbf{i}_{\alpha\beta}^p[k+2] = \mathbf{i}_{\alpha,\beta}[k] + \Delta\mathbf{i}_{\alpha,\beta}\Big|_{S^k}^{T_s} + \Delta\mathbf{i}_{\alpha,\beta}\Big|_{S^{k+1}}^{T_s}. \tag{5}$$

The first term, $\mathbf{i}_{\alpha,\beta}[k]$, can be measured from the initial current sampling, while the second and third terms, $\Delta\mathbf{i}_{\alpha,\beta}\big|_{S^k}^{T_s}$ and $\Delta\mathbf{i}_{\alpha,\beta}\big|_{S^{k+1}}^{T_s}$, are the current differences at the end of switching intervals of $(k+1)th$ and $(k+2)th$, respectively.

As revealed by (5), the prediction of future stator currents is highly susceptible to the accuracies of the current differences depicted by (3) and (4). Similarly, the current difference of the switching interval of $(k-1)th$ can be calculated by

$$\Delta\mathbf{i}_{\alpha,\beta}\Big|_{S^{k-1}}^{T_s} = \mathbf{i}_{\alpha,\beta}[k] - \mathbf{i}_{\alpha,\beta}[k-1]. \tag{6}$$

The switching states S^{k-1}, S^k and S^{k+1} in (3)-(6) belong to one of the four switching states. During each sampling period, the value of (6) is stored to update the current difference corresponding to the same switching state. If their respective switching states match, the latest stored value will be used to predict the values of (3) and (4). In this way, the MFPCC can effectively reduce the dependency and sensitivity of current predictions on motor parameters and extended back-EMF compared to the MPCC of (2). The MFPCC also accounts for the delay compensation in expanding the prediction horizon to $k+2$. However, it is worth noting that the updating frequency of (3)-(4) and (6) must be high enough to minimize the prediction error.

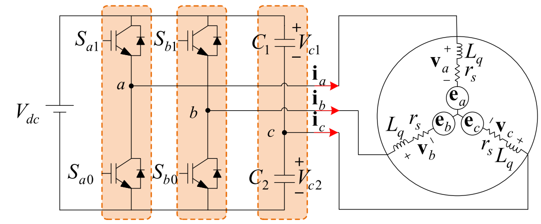

FIGURE 1. The general architecture of an FSTP inverter-fed SynRM.

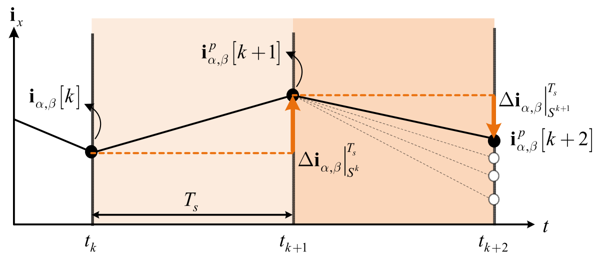

FIGURE 2. Schematic diagram of current prediction in the MFPCC [29] applied to the FSTPI.

Moreover, offset in the capacitor voltage of the FSTP inverter caused by load current disturbances is less significant under balanced voltage. Theoretically, the sum of the stator currents is zero, *i.e.*, $\mathbf{i}_a + \mathbf{i}_b + \mathbf{i}_c = 0$ for a three-phase balanced system. Technically, the nonparametric nature of the MFPCC makes the control scheme largely simplified *via* sensing currents on the two active phases of the FSTP inverter. As a result, $\mathbf{i}_c$ can be directly calculated by (7),

$$\begin{cases} \mathbf{i}_c = C_1 \dfrac{dV_{c1}}{dt} - C_2 \dfrac{dV_{c2}}{dt} \\ \quad = -\mathbf{i}_a - \mathbf{i}_b. \end{cases} \tag{7}$$

III. THE PROPOSED MMFPCC

A. ADAPTIVE APPLICATION TIME

The conventional MFPCC only applies a single switching state at a fixed duration in every sampling period, yielding large current ripples [28]. In the case of FSTPI, the problem makes even more challenging because of its architecture with only four switching voltage vectors available. As shown in Fig. 3, the four basic voltage vectors are denoted as v_1, v_2, v_3, and v_4.

To boost the candidate voltage vectors, six modulated voltage vectors labeled as v_1^m, v_2^m, v_3^m, v_4^m, v_5^m, and v_6^m is synthesized in the proposed method. Each modulated voltage vector is composed of two basic voltage vectors with different durations, *i.e.* application times. Suppose the two durations in the $(k+1)th$ sampling period are T_1^{k+1} and T_2^{k+1}, for instance, with their sum equaling to the period T_s

$$T_1^{k+1} + T_2^{k+1} = T_s. \tag{8}$$

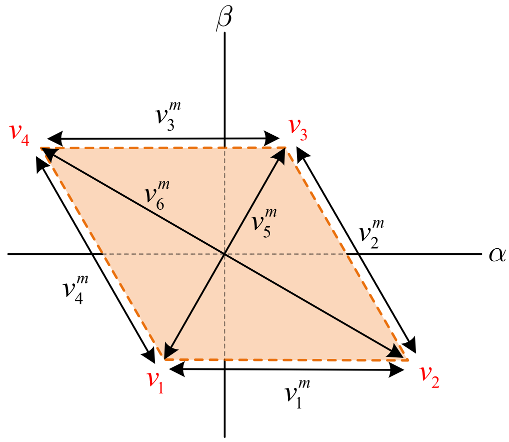

FIGURE 3. Diagram of voltage space vector of the proposed scheme.

Dividing both sides by T_s, one gets the following expression

$$D_1^{k+1} + D_2^{k+1} = 1, \tag{9}$$

where $D_1^{k+1} = T_1^{k+1}/T_s$ and $D_2^{k+1} = T_2^{k+1}/T_s$ represent the first and the second duty ratios, respectively. The optimal duty ratio (superscripted by "opt" in the sequel) $D_1^{\mathrm{opt},k+1}$ can be obtained through the following identity,

$$\frac{\partial g}{\partial D_1^{k+1}} = 0, \tag{10}$$

where "g" is the so-called cost function that serves as a performance measure yet to be defined. Based on the design criteria (8)-(9), the second optimal duty ratio can be simply calculated *via* $D_2^{\mathrm{opt},k+1} = (1 - D_1^{\mathrm{opt},k+1})$, meaning that the two optimal duty ratios must complement each other. Details of the modulated voltage vector combinations can be seen in Table 1, which can be generally expressed as

$$v_w^m [k+1] = v_x D_1^{k+1} + v_y D_2^{k+1} \tag{11}$$

where $w \in \{1, \cdots, 6\}$ and $x \neq y \in \{1, 2, 3, 4\}$. In this context, the term "adaptive" depicts the adaptability feature of the proposed method in detecting stator currents of the switching vectors.

B. ADAPTIVE CURRENT DETECTION

The stator current and current differences are measured and calculated within a sampling period in the conventional MFPCC [28]. In general, fixed and equal application time is adopted. In contrast to [28], the new strategy employs a two-vector-based switching and uses an adaptive scheme to detect current.

As depicted in Fig. 4, the switching mode S_k^m, consisting of two switching states S_1^k and S_2^k, is applied in the $(k)th$ sampling period. The corresponding durations are denoted as T_1^k and T_2^k, respectively. It is worth noting that the variables S_k^m, S_1^k, S_2^k, T_1^k, and T_2^k are calculated and determined in the $(k\text{-}1)th$ sampling period but applied at the $(k)th$ period. The first stator current, denoted as $\mathbf{i}_x [k, 1]$, is sampled after a short time delay from the moment the first switching state S_1^k is applied to avoid the current surge resulting from inverter switching. To be more specific, a short delay is configured between the switching and sampling points using the enhanced pulse width modulator (ePWM) peripheral of the microcontroller, approximately equaling to 4μs. The same policy applies to the second current sampling, which is denoted as $\mathbf{i}_x [k, 2]$. As shown in Fig. 4, the current difference corresponding to the first switching state S_1^k with the application time T_1^k can be calculated from the two successive current measurements,

$$\Delta \mathbf{i}_x^{\mathrm{new}} \Big|_{S_1^k}^{T_1^k} = \mathbf{i}_x [k, 2] - \mathbf{i}_x [k, 1] \tag{12}$$

where the superscript "new" refers to the newly calculated value, and the subscript "x" represents phase α or β. Similarly, the stator current $\mathbf{i}_x [k-1, 2]$ is measured by the end of the switching state S_2^{k-1} in the $(k\text{-}1)th$ period. The current difference between $\mathbf{i}_x [k, 1]$ and $\mathbf{i}_x [k-1, 2]$ is

$$\Delta \mathbf{i}_x^{\mathrm{new}} \Big|_{S_2^{k-1}}^{T_2^{k-1}} = \mathbf{i}_x [k, 1] - \mathbf{i}_x [k-1, 2]\,. \tag{13}$$

TABLE 1. The relationship between the switching mode and the modulated voltage vector.

Switching Mode	Vector Combination	S_1^{k+1}	S_2^{k+1}	Modulated Voltage Vector
S_1^m	$v_1 D_1^{k+1} + v_2 D_2^{k+1}$	$S_1(00)$	$S_2(10)$	v_1^m
S_2^m	$v_2 D_1^{k+1} + v_3 D_2^{k+1}$	$S_2(10)$	$S_3(11)$	v_2^m
S_3^m	$v_3 D_1^{k+1} + v_4 D_2^{k+1}$	$S_3(11)$	$S_4(01)$	v_3^m
S_4^m	$v_4 D_1^{k+1} + v_1 D_2^{k+1}$	$S_4(01)$	$S_1(00)$	v_4^m
S_5^m	$v_1 D_1^{k+1} + v_3 D_2^{k+1}$	$S_1(00)$	$S_3(11)$	v_5^m
S_6^m	$v_2 D_1^{k+1} + v_4 D_2^{k+1}$	$S_2(10)$	$S_4(01)$	v_6^m

As can be seen from (12) and (13), the two current differences are related to both the switching states and their application times. The application time is fixed in [28], [29], whose current difference is only relevant to different switching states. Compared to these earlier methods [28], [29], one of the technical advantages of the new scheme is that its application durations are adaptive and the duty ratios are optimized.

C. CURRENT DIFFERENCE MODIFICATION

The common drawback of the MPCC is its dependency on model parameters, as can be seen from (8). Parameter variations and mismatches will naturally result in unsatisfactory performances, leading to large current tracking errors. The model-free predictive current control (MFPCC) provides a good solution to resolve the difficulty [25].

It is assumed in [29] that current differences under the same switching state between consecutive sampling periods have similar values. Therefore, the latest current difference data can be used to predict future ones, provided their corresponding switching states are the same. However, it becomes inapplicable if the duty ratio is varying, as shown in Fig. 4.

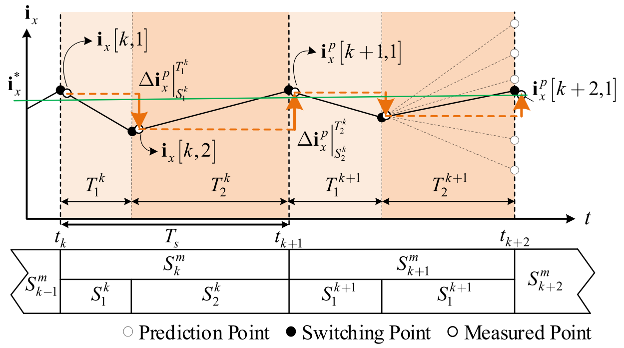

FIGURE 4. Schematic illustration of stator current prediction points of the proposed MMFPCC.

Note that the application times corresponding to (12) and (13) can differ. A solution is proposed here to solve the problem of predicting current differences at different application times. The current differences associated with the switching states S_2^{k-1} and S_1^k can be respectively predicted as follows:

$$\Delta \mathbf{i}_x^m\Big|_{S_2^{k-1}}^{T_s} = \Delta \mathbf{i}_x^{\mathrm{old}}\Big|_{S_2^{k-1}}^{T_1^{k-1}} + \Delta \mathbf{i}_x^{\mathrm{new}}\Big|_{S_2^{k-1}}^{T_2^{k-1}} = D_{k-1}^1 \cdot \Delta \mathbf{i}_x^{\mathrm{old}}\Big|_{S_2^{k-1}}^{T_s} + \mathbf{i}_x[k,1] - \mathbf{i}_x[k-1,2] \tag{14}$$

$$\Delta \mathbf{i}_x^m\Big|_{S_1^k}^{T_s} = \Delta \mathbf{i}_x^{\mathrm{new}}\Big|_{S_1^k}^{T_1^k} + \Delta \mathbf{i}_x^{\mathrm{old}}\Big|_{S_1^k}^{T_2^k} = \mathbf{i}_x[k,2] - \mathbf{i}_x[k,1] + D_2^k \cdot \Delta \mathbf{i}_x^{\mathrm{old}}\Big|_{S_2^k}^{T_s} \tag{15}$$

where the superscript "m" stands for the "modified" current difference, D_1^{k-1} denotes the first duty ratio in the (k-1)*th* sampling period, D_2^k refers to the second duty ratio in the (k)*th* sampling period, the superscript "old" represents the old value, and S_2^{k-1}, S_1^k, $S_2^k \in \{S_1, S_2, S_3, S_4\}$. As depicted by (14), the symbols $\Delta \mathbf{i}_x^{\mathrm{old}}\big|_{S_2^{k-1}}^{T_1^{k-1}}$ and $\Delta \mathbf{i}_x^{\mathrm{old}}\big|_{S_2^{k-1}}^{T_s}$ indicate that the old current differences stored in the microcontroller are derived from the same switching state of S_2^{k-1} and different application times T_1^{k-1} and T_s, respectively. The modified current difference $\Delta \mathbf{i}_x^m\big|_{S_2^{k-1}}^{T_s}$ in (14) can be calculated from the two successive current differences within a given sampling period known as the "old" and "new" values. After the execution of (14) and (11) in sequence, the current difference $\Delta \mathbf{i}_x^m\big|_{S_1^k}^{T_s}$ corresponding to the switching state S_1^k and the application time T_s can be obtained *via* (15).

Since the accuracy of the current difference plays a significant role in the MFPCC, the old current difference must be updated within each sampling period. However, the update frequency of the old current difference in [29] is one in every sampling period, whereas the new scheme provides two updates as follows:

$$\Delta \mathbf{i}_x^{\mathrm{old}}\Big|_{S_2^{k-1}}^{T_s} \rightarrow \Delta \mathbf{i}_x^m\Big|_{S_2^{k-1}}^{T_s} \tag{16}$$

$$\Delta \mathbf{i}_x^{\mathrm{old}}\Big|_{S_1^k}^{T_s} \rightarrow \Delta \mathbf{i}_x^m\Big|_{S_1^k}^{T_s}. \tag{17}$$

D. CURRENT PREDICTION WITH OPTIMIZED DUTY RATIO

As described in (9), the current difference can be affected by its measurement characteristics. In short, duty ratios follow $D_2^k = (1 - D_1^k)$ and $D_2^{k+1} = (1 - D_1^{k+1})$. As such, the current difference $\Delta \mathbf{i}_x^p\big|_{S_1^k}^{T_1^k}$ described in Fig. 4 is defined as

$$\Delta \mathbf{i}_x^p\Big|_{S_1^k}^{T_1^k} = D_1^k \cdot \Delta \mathbf{i}_x^{\mathrm{old}}\Big|_{S_1^k}^{T_s} \tag{18}$$

where $D_1^k = T_1^k / T_s$ is the first duty ratio. Similarly, the second current difference $\Delta \mathbf{i}_x^p\big|_{S_2^k}^{T_2^k}$ is predicted by

$$\Delta \mathbf{i}_x^p\Big|_{S_2^k}^{T_2^k} = D_2^k \cdot \Delta \mathbf{i}_x^{\mathrm{old}}\Big|_{S_2^k}^{T_s} = \left(1 - D_1^k\right) \cdot \Delta \mathbf{i}_x^{\mathrm{old}}\Big|_{S_2^k}^{T_s}. \tag{19}$$

Following (18) and (19), the predicted future current differences at $(k+1)th$ switching interval $\Delta \mathbf{i}_x^p\big|_{S_1^{k+1}}^{T_1^{k+1}}$ and $\Delta \mathbf{i}_x^p\big|_{S_2^{k+1}}^{T_2^{k+1}}$ can be calculated by the equations

$$\Delta \mathbf{i}_x^p\Big|_{S_1^{k+1}}^{T_1^{k+1}} = D_1^{k+1} \cdot \Delta \mathbf{i}_x^{\mathrm{old}}\Big|_{S_1^{k+1}}^{T_s} \tag{20}$$

$$\Delta \mathbf{i}_x^p\Big|_{S_2^{k+1}}^{T_2^{k+1}} = D_2^{k+1} \cdot \Delta \mathbf{i}_x^{\mathrm{old}}\Big|_{S_2^{k+1}}^{T_s} = \left(1 - D_1^{k+1}\right) \cdot \Delta \mathbf{i}_x^{\mathrm{old}}\Big|_{S_2^{k+1}}^{T_s} \tag{21}$$

where S_1^{k+1}, $S_2^{k+1} \in \{S_1, S_2, S_3, S_4\}$. After executing (16) and (17), previous current differences corresponding to the applied time T_s can then be linearly adjusted to predict other current differences at different application times accordingly. As such, all current differences shown in Fig. 4 become predictable. Moreover, to account for the time delay compensation together with (18)-(21), one concludes that the $(k+2)th$ current prediction can be expressed as

$$\mathbf{i}_x^p[k+2,1] = \mathbf{i}_x[k,1] + \Delta \mathbf{i}_x^p\Big|_{S_1^k}^{T_1^k} + \Delta \mathbf{i}_x^p\Big|_{S_2^k}^{T_2^k} + \Delta \mathbf{i}_x^p\Big|_{S_1^{k+1}}^{T_1^{k+1}} + \Delta \mathbf{i}_x^p\Big|_{S_2^{k+1}}^{T_2^{k+1}}. \tag{22}$$

where the subscript "x" refers to the α-axis and β-axis. We now formally define the cost function "g" as

$$g = \left(\mathbf{i}_\alpha^*[k] - \mathbf{i}_\alpha^p[k+2,1]\right)^2 + \left(\mathbf{i}_\beta^*[k] - \mathbf{i}_\beta^p[k+2,1]\right)^2 \tag{23}$$

where the superscript "$*$" refers to the current command. The difference between the current command and the predicted values, namely, the current error, is denoted by $\varepsilon_{\alpha,\beta}$. The cost function (23) can be rewritten accordingly as

$$g = \left(C_{\alpha 1} + D_1^{k+1} C_{\alpha 2}\right)^2 + \left(C_{\beta 1} + D_1^{k+1} C_{\beta 2}\right)^2 \tag{24}$$

where $C_{\alpha 1}$, $C_{\alpha 2}$, $C_{\beta 1}$, and $C_{\beta 2}$ are defined as follows:

$$C_{\alpha 1} = \mathbf{i}_\alpha^*[k] - \mathbf{i}_\alpha[k,1] - \Delta \mathbf{i}_\alpha^p\Big|_{S_1^k}^{T_1^k} - \Delta \mathbf{i}_\alpha^p\Big|_{S_2^k}^{T_2^k} - \Delta \mathbf{i}_\alpha^{\mathrm{old}}\Big|_{S_2^{k+1}}^{T_s} \tag{25}$$

$$C_{\alpha 2} = \Delta \mathbf{i}_\alpha^{\mathrm{old}}\Big|_{S_2^{k+1}}^{T_s} - \Delta \mathbf{i}_\alpha^{\mathrm{old}}\Big|_{S_1^k}^{T_s} \tag{26}$$

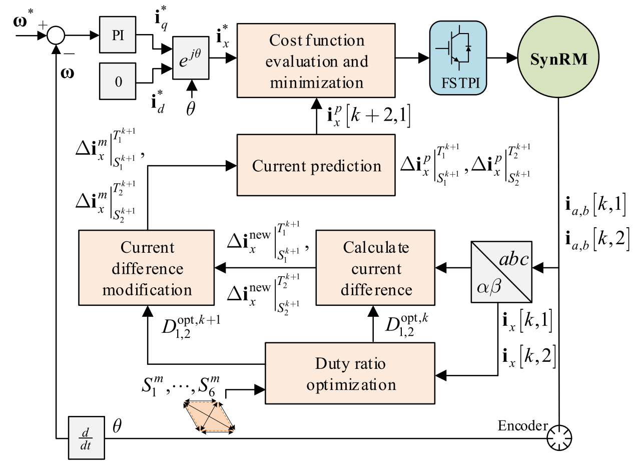

FIGURE 5. Control diagram of the proposed MMFPCC.

$$C_{\beta 1} = \mathbf{i}_\beta^*[k] - \mathbf{i}_\beta[k,1] - \Delta \mathbf{i}_\beta^p\Big|_{S_1^k}^{T_1^k} - \Delta\mathbf{i}_\beta^p\Big|_{S_2^k}^{T_2^k} - \Delta\mathbf{i}_\beta^{\mathrm{old}}\Big|_{S_2^{k+1}}^{T_s} \tag{27}$$

$$C_{\beta 2} = \Delta\mathbf{i}_\beta^{\mathrm{old}}\Big|_{S_2^{k+1}}^{T_s} - \Delta\mathbf{i}_\beta^{\mathrm{old}}\Big|_{S_1^{k}}^{T_s}. \tag{28}$$

Assume (24) is a continuous and differentiable function. To get the optimal duty ratio, we let $\frac{\partial g}{\partial D_1^{k+1}} = 0$and obtain

$$2C_{\alpha 2}\left(C_{\alpha 1}+D_1^{k+1}C_{\alpha 2}\right)+2C_{\beta 2}\left(C_{\beta 1}+D_1^{k+1}C_{\beta 2}\right)=0. \tag{29}$$

$$D_1^{\mathrm{opt},k+1} = \frac{-C_{\alpha 1}C_{\alpha 2} - C_{\beta 1}C_{\beta 2}}{\left(C_{\alpha 2}\right)^2 + \left(C_{\beta 2}\right)^2}. \tag{30}$$

For practical reasons such as hardware limitations of the drive system and to prevent the input voltage vectors from overlapping within a period, a constraint is imposed as $0.2 \leq D_1^{\mathrm{opt},k+1} \leq 0.8$ amid implementation. The duty ratio will be replaced by 0.2 or 0.8, respectively, when it falls below 0.2 or goes above 0.8. This optimal duty ratio will be executed D_1^{k+1} as in (20) and (21). The current prediction equation of (22) is rewritten now as

$$\begin{aligned}\mathbf{i}_x^p[k+2,1] &= \mathbf{i}_x[k,1] + D_1^k \cdot \Delta\mathbf{i}_x^{\mathrm{old}}\Big|_{S_1^k}^{T_s} + \left(1-D_1^k\right)\cdot\Delta\mathbf{i}_x^{\mathrm{old}}\Big|_{S_2^k}^{T_s} \\ &\quad + D_1^{\mathrm{opt},k+1}\cdot\Delta\mathbf{i}_x^{\mathrm{old}}\Big|_{S_1^{k+1}}^{T_s} + \left(1-D_1^{\mathrm{opt},k+1}\right)\cdot\Delta\mathbf{i}_{\mathbf{x}}^{\mathrm{old}}\Big|_{S_2^{k+1}}^{T_s}.\end{aligned} \tag{31}$$

As illustrated in Fig. 4, the respective future predicted currents corresponding to the six modulated voltage vectors can be obtained *via* (31). Fig. 5 describes the five fundamental processes involved in the workflow of the proposed new scheme. It begins by measuring the currents and calculating the current difference between consecutive switching intervals. Then, the optimal duty ratios are obtained to modify and optimize the calculated current difference. Current predictions corresponding to all 6 candidate switching modes are performed, and the one that minimizes the cost function is considered the best and applied in the next control cycle.

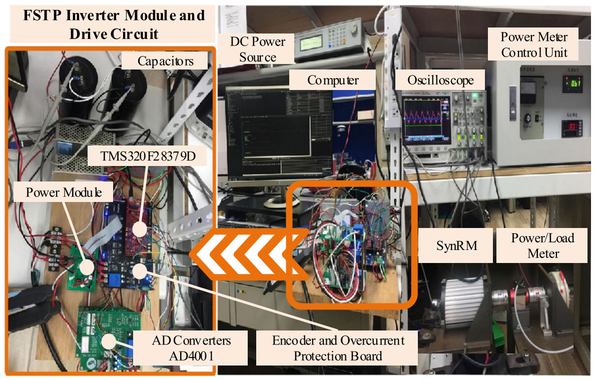

FIGURE 6. Experimental setup and hardware components.

TABLE 2. Machine and system parameters.

Parameter	Unit	Value
Rated power	W	500
Rated torque	Nm	2
Rated speed	rpm	1500
Number of poles	pole	4
Stator resistance	Ω	2.5
d-axis inductance	*m*H	40
q-axis inductance	*m*H	16
DC-bus voltage	V	200
Control period	μs	100

IV. EXPERIMENTAL VALIDATION AND PERFORMANCE ASSESSMENT

Fig. 6 shows a prototype SynRM drive system equipped with a 32-bit floating-point microcontroller, TMS320F28379D, is built to realize and validate the new scheme. Specifications of the SynRM are provided in Table 2. The FSTP inverter module is connected with two capacitors at a rated capacitance of 10,000μF and a rated voltage of 400V. Two current sensors (AD4001) are installed to collect data through a differential encoder connected to the drive circuit board. Analysis and data processing is performed using the software MATLAB®. For fair comparisons, both the new approach and the existing MFPCC [29] are subject to the same conditions in all experiments.

A. FEASIBILITY AND RESPONSES

Illustrated in Fig. 7 is the current signal obtained from the DSOX3034A digital oscilloscope by Keysight. Thanks to the interrupt service routine implemented on the TMS320F28379D microcontroller, adaptive current detection can be realized and proved to be feasible. The scheme's adaptivity can be observed in terms of the applied durations and the stator current detections. The short time delay between the switching point and the sampling point is evident, as shown therein. From the same figure, one can easily observe that the inverter indeed switches twice in a sampling period, executing two switching with variable durations.

Meanwhile, it is observed that the increase of input voltage vectors in the new scheme has resulted in more average computation time than that of the non-adaptive counterpart

TABLE 3. Sampling period and computation time.

Method	Sampling Period (T_s)	Average Computation Time
MFPCC [29]	100 μs	20.53 μs
Proposed MMFPCC	100 μs	36.17 μs

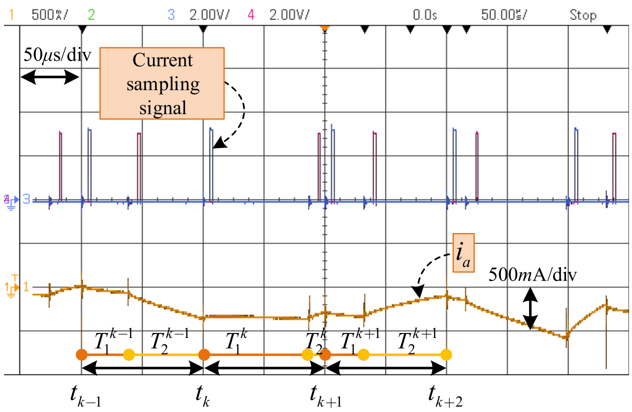

FIGURE 7. Measurements of stator current in phase-a and the related sampling signal.

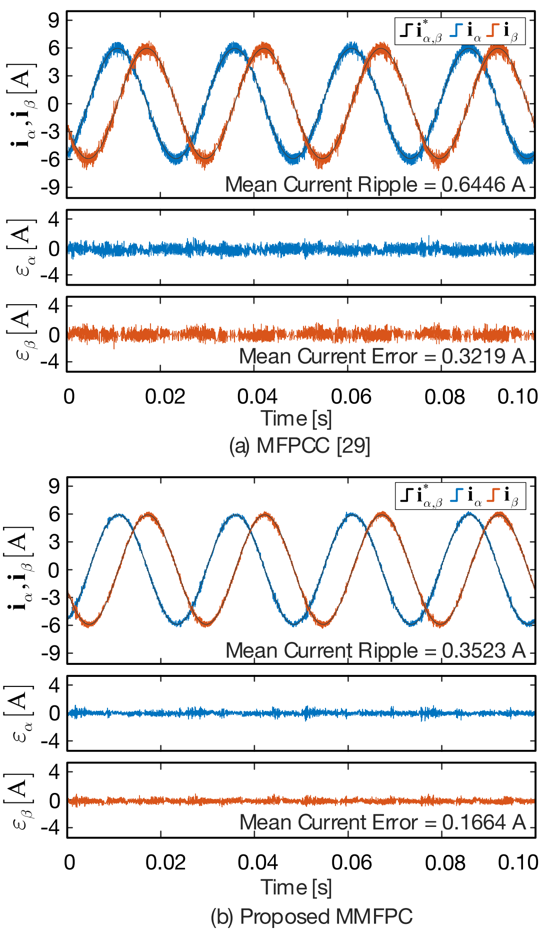

FIGURE 8. Steady-state waveforms of stator current under a command of 6 A and a frequency of 10 Hz. From top to bottom: actual current response and current errors.

MFPCC [29]. Table 3 lists the average execution time of the two methods, denoting the calculation time required for the controller to perform cost evaluation and current prediction. An interrupt service routine is used in the ePWM to calculate the processing time for the main loop to solve the control problem. The real-time execution can be viewed from the code composer studio (CCS) or measured *via* an oscilloscope. The results show that the conventional method used an average time of 20.53 μs compared to 36.17 μs of the proposed one, which implies an increase of 76.18% computational burden. This is expected because the number of input vectors is doubled. In particular, the proposed new scheme involves an additional optimization process for the duty ratios, requiring more computations. The trade-off in gaining significant improvements on the prediction accuracy is higher computational complexity and loading, yet fortunately without sacrificing too much on the controller's capacity.

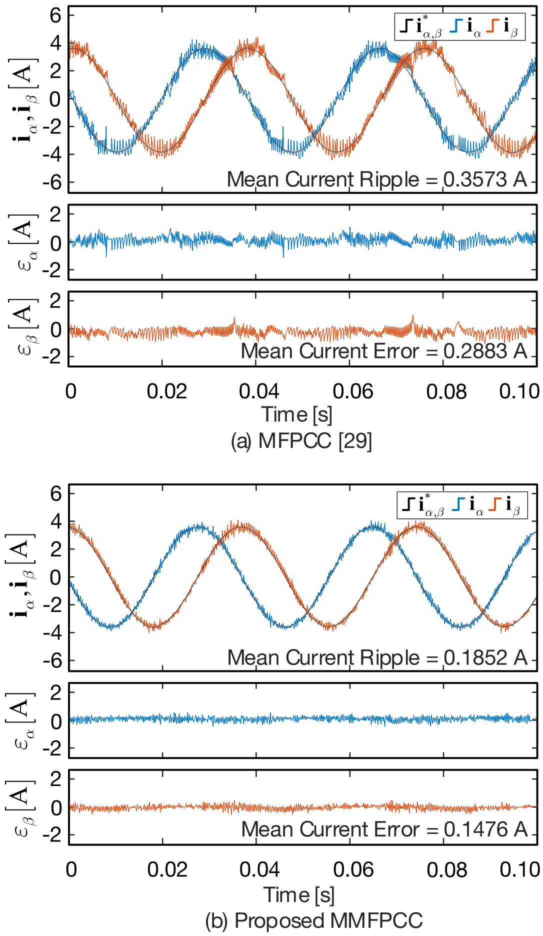

FIGURE 9. Steady-state waveforms of stator current under a speed command of 800 rpm and an external load-torque of 2.5 Nm. From top to bottom: actual current response and current errors.

B. STEADY-STATE PERFORMANCE ASSESSMENT

As shown in Fig. 8 to Fig. 12, the steady-state performance of current tracking is evaluated by two tests under different current and speed commands. An external load-torque is also introduced to assess the performance under strain conditions. The computed mean values of current ripples, current errors,

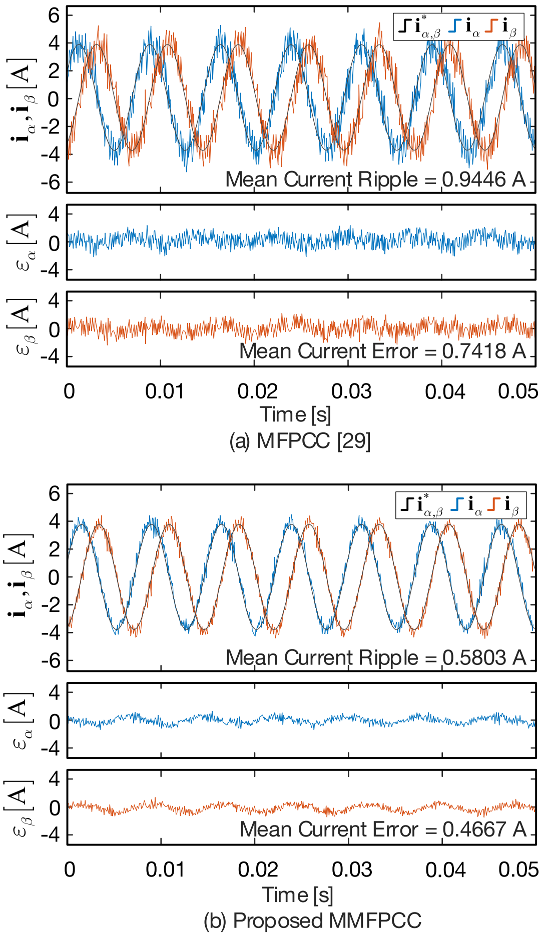

FIGURE 10. Steady-state waveforms of stator current under a speed command of 2000 rpm and an external load-torque of 2.5 Nm. From top to bottom: actual current response and current errors.

and total harmonic distortions (THD) are taken as the performance assessment measures.

1) PERFORMANCE OF CURRENT TRACKING

The measured stator currents are provided in Figs. 8 to 10 under different commands. Illustrated in Fig. 8 are the α-β current responses from a current command of 6 A and a frequency of 10 Hz. Both the existing MFPCC [29] and the proposed MMFPCC exhibit excellent current tracking capabilities, as revealed by Figs. 8(a) and 8(b), respectively, mainly thanks to their model-free nature. Quantitatively, the mean current ripple and the mean current error of the proposed MMFPCC are reduced by 0.6446 A and 0.3523 A, respectively, when compared to MFPCC [29]. Another experiment was performed to evaluate the current response under a speed command of 800 rpm and a high speed of 2000 rpm, both under a load-torque disturbance of 2.5 Nm. Since the external load-torque set in Fig. 9 and 10 is larger than the motor's rated torque of 2 Nm, the overloading condition induces more current ripples. It can be observed from the current waveforms from Fig. 9 that the proposed MMFPCC effectively reduces the mean current ripple and the mean current error over the conventional MFPCC [29] by 48.17% and 48.80%, respectively. As revealed by Fig. 10, the impact from overloading is more evident at a higher speed, with the conventional MFPCC [29] suffers from larger and heavier current ripples. The proposed new scheme, on the other hand, effectively alleviates current errors, which is a good indication that the prediction strategy indeed works efficiently.

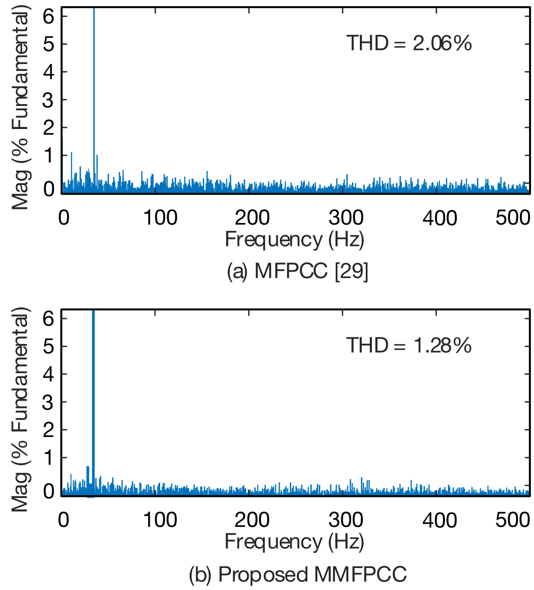

FIGURE 11. Harmonic spectrum under a current command of 6 A and a frequency of 10 Hz.

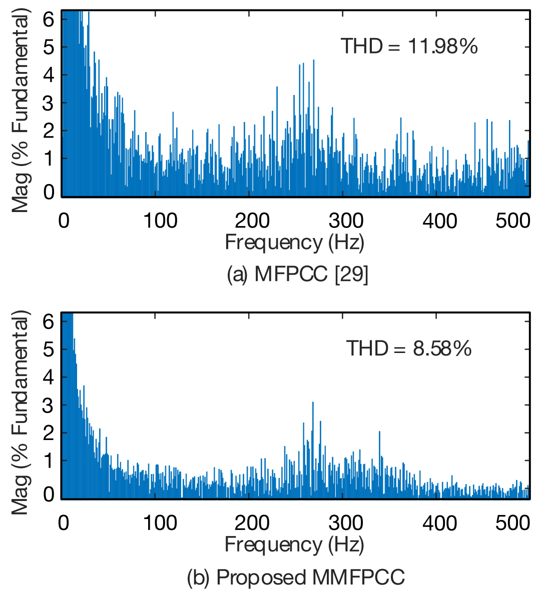

FIGURE 12. Harmonic spectrum under a speed command of 800 rpm and a load-torque disturbance of 2.5 Nm.

2) PHASE HARMONIC PROFILE

The total harmonic distortion (THD) is taken to be a performance measure to further assess the steady-state response. Shown in Figs. 11-12 is the Fast Fourier Transform (FFT) applied to the α-axis stator currents of Figs. 8-9, respectively. It can be seen from Fig. 11 that the THD is 2.06% of the

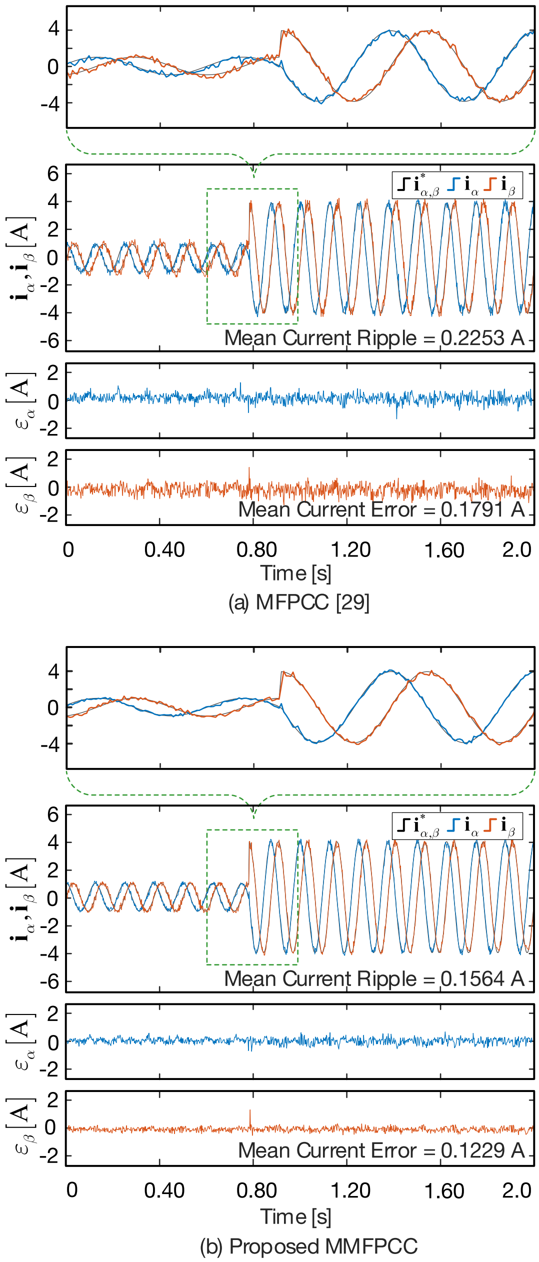

FIGURE 13. Dynamic performance of stator current under a current jump from 1 A to 4 A under a load-torque of 0.6 Nm. From top to bottom: actual current response with a section enlarged and current errors.

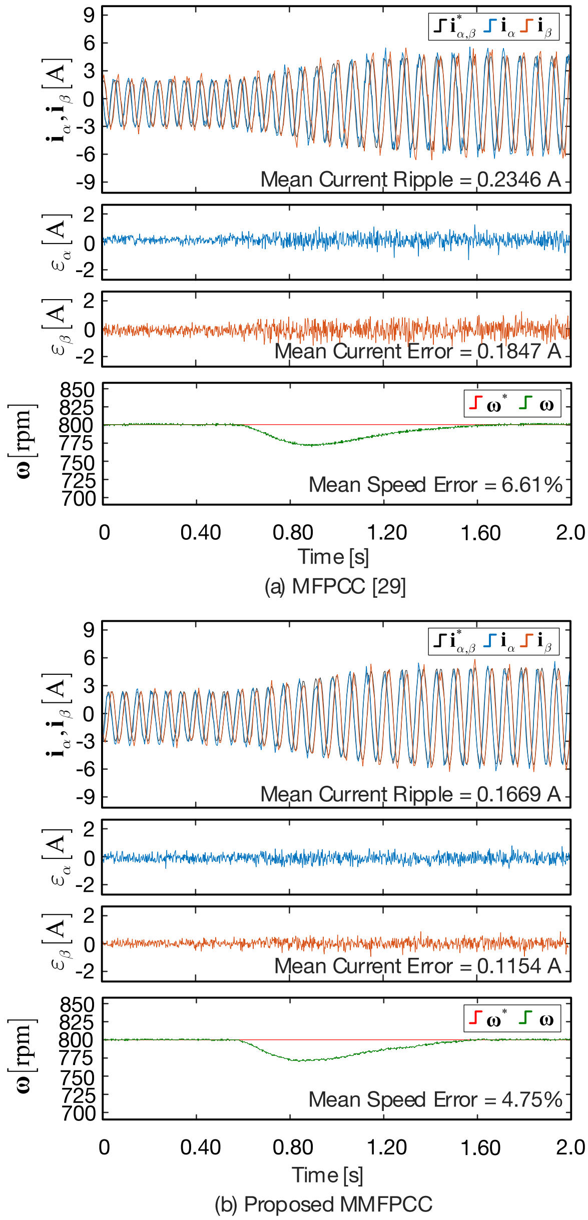

FIGURE 14. Dynamic performance of stator current from a progressively varying load-torque from 0.6 Nm to 1.5 Nm under a constant speed of 800 rpm. From top to bottom: actual current response, current errors and speed response.

MFPCC [29] and 1.28% of the proposed MMFPCC. In the case of an overloading condition, as shown in Fig. 12, the harmonic spectrum's noise is more evident at some frequencies, particularly more so in Fig. 12(a) than in Fig. 12(b). The THD of the stator currents is 11.98% and 8.58% for the conventional MFPCC [29] and the proposed MMFPCC, respectively, suggesting the THD is significantly reduced by 28.38%. Such results prove the fact that the scheme benefits a lot from integrating variable durations into the MFPCC, which yields a lower current harmonic distortion. The latter is expected and verified by the experimental results of Figs. 11-12.

C. PERFORMANCE IN TERMS OF TRANSIENT RESPONSE

This section presents the transient response of the controllers under different operating commands. Both methods are subjected to the following tests: jump current command, step load-torque, and step speed command.

1) JUMP CURRENT COMMAND AND RESPONSE

In this test, a current command jumping from 1 A to 4 A is applied at about 0.8 sec. The motor operates at a load-torque command of 0.6 Nm. As can be seen from Fig. 13, both controllers produce good responses. However, by inspecting the enlarged green dotted box in the same figure, one may see a significant difference in current tracking capability. Scattered

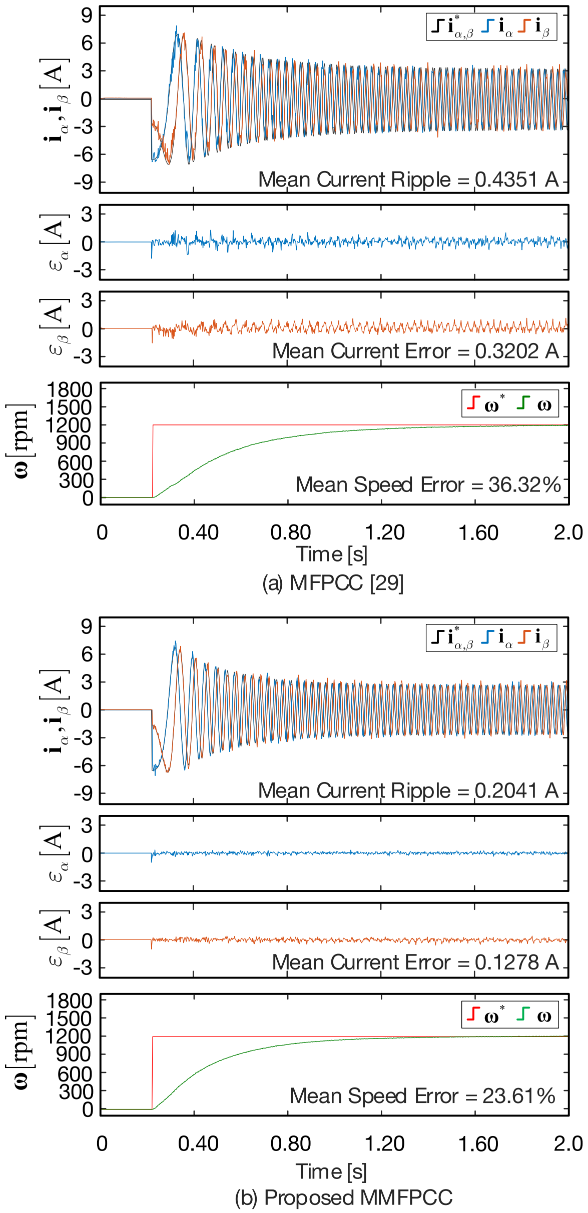

FIGURE 15. Dynamic performance of stator currents under a step speed command from 0 rpm to 1200 rpm. From top to bottom: current response, current errors and speed response.

and pulsating current spikes are visible in the conventional MFPCC [29] but are not so in the new scheme as the latter exhibits a smoother step response and lesser distortions. The mean current ripple of the MFPCC is 0.2253 A as opposed to 0.1564 A of the new scheme. Specifically, the mean current ripple and mean current error are effectively reduced by 30.58% and 31.38%, respectively.

2) PROGRESSIVE LOAD-TORQUE VARIATION AND RESPONSE

Fig. 14 shows the two controllers' performance with the motor running at a constant speed of 800 rpm while undergoing a progressive load-torque variation from 0.6 Nm to 1.5 Nm. The stator currents are effectively controlled, but a significant current ripple is observed due to the increasing load effect. Quantitatively, the mean current ripple and mean current error of the proposed MMFPPC are respectively reduced by 28.86% and 37.52% compared to that of the conventional MFPCC [29]. The changes in the load-torque also affected the speed tracking performance of the SynRM. The speed slowed down, exhibiting a drooping effect in its trajectory but recovered immediately within a brief period. Furthermore, the mean speed error is significantly reduced from 6.61% of the existing MFPCC [29] to 4.75% of the proposed method.

3) STEP SPEED COMMAND AND RESPONSE

A step speed command is given to evaluate the current response and the speed response. For a fair comparison, both controllers use the same controller in the speed loop, which is of proportional-integral (PI) type. Fig. 15 shows the current tracking performance under a step speed command from 0 rpm to 1200 rpm. The mean current ripples of the MFPCC is 0.4351 A, whereas the proposed MMFPCC is 0.2041 A. Moreover, the mean speed errors of MFPCC is 36.32%, in contrast to 23.61% from the MMFPCC. Results revealed that the proposed new scheme has better performance in current prediction and speed response compared to its non-adaptive predecessor.

V. CONCLUSION

A modulated model-free predictive current control (MMFPCC) is proposed in this paper to improve the performance of a SynRM drive system powered by an FSTP inverter. Six new modulated switching modes are obtained by synthesizing two basic voltage vectors and adaptive optimal duty ratios. The calculated current differences are adaptively corrected according to their applied durations, thereby largely enhancing the current prediction accuracies. Finally, the presented experimental results demonstrated a significant performance improvement on the motor drive in terms of the mean current ripples, the mean current errors, and the THD under steady-state and dynamic operating conditions. Compared to its non-adaptive counterpart, the new scheme provides a much more effective and feasible solution for current predictions.

REFERENCES

[1] E. Daryabeigi and S. Vaez-Zadeh, "A combined control for fast and smooth performance of IPM motor drives over wide operating conditions," *IEEE Trans. Energy Convers.*, vol. 33, no. 3, pp. 1384–1391, Sep. 2018, doi: 10.1109/TEC.2018.2810202.

[2] M. Hinkkanen, H. A. A. Awan, Z. Qu, T. Tuovinen, and F. Briz, "Current control for synchronous motor drives: Direct discrete-time pole-placement design," *IEEE Trans. Ind. Appl.*, vol. 52, no. 2, pp. 1530–1541, Mar./Apr. 2016, doi: 10.1109/TIA.2015.2495288.

[3] F. Oliveira and A. Ukil, "Comparative performance analysis of induction and synchronous reluctance motors in chiller systems for energy efficient buildings," *IEEE Trans. Ind. Informat.*, vol. 15, no. 8, pp. 4384–4393, Aug. 2019, doi: 10.1109/TII.2018.2890270.

[4] A. Fratta and A. Vagati, "A reluctance motor drive for high dynamic performance application," *IEEE Trans. Ind. Appl.*, vol. 28, no. 4, pp. 873–879, Jul./Aug. 1992, doi: 10.1109/28.148454.

[5] A. T. de Almeida, F. J. T. E. Ferreira, and G. Baoming, "Beyond induction motors—Technology trends to move up efficiency," *IEEE Trans. Ind. Appl.*, vol. 50, no. 3, pp. 2103–2114, May/Jun. 2014, doi: 10.1109/TIA.2013.2288425.

[6] L. Huber, M. Kumar, and M. M. Jovanović, "Performance comparison of three-step and six-step PWM in average-current-controlled three-phase six-switch boost PFC rectifier," *IEEE Trans. Power Electron.*, vol. 31, no. 10, pp. 7264–7272, Oct. 2016, doi: 10.1109/TPEL.2015.2506554.

[7] B. Mirafzal, "Survey of fault-tolerance techniques for three-phase voltage source inverters," *IEEE Trans. Ind. Electron.*, vol. 61, no. 10, pp. 5192–5202, Oct. 2014, doi: 10.1109/TIE.2014.2301712.

[8] K. Ni, Y. Hu, G. Chen, C. Gan, and X. Li, "Fault-tolerant operation of DFIG-WT with four-switch three-phase grid-side converter by using simplified SVPWM technique and compensation schemes," *IEEE Trans. Ind. Appl.*, vol. 55, no. 1, pp. 659–669, Jan./Feb. 2019, doi: 10.1109/TIA.2018.2866483.

[9] C. A. Agustin, J.-T. Yu, C.-K. Lin, J. Jai, and Y.-S. Lai, "Triple-voltage-vector model-free predictive current control for four-switch three-phase inverter-fed SPMSM based on discrete-space-vector modulation," *IEEE Access*, vol. 9, pp. 60352–60363, 2021, doi: 10.1109/ACCESS.2021.3074067.

[10] D. Zhou, X. Li, and Y. Tang, "Multiple-vector model-predictive power control of three-phase four-switch rectifiers with capacitor voltage balancing," *IEEE Trans. Power Electron.*, vol. 33, no. 7, pp. 5824–5835, Jul. 2018, doi: 10.1109/TPEL.2017.2750766.

[11] B. Wang, J. Hu, and W. Hua, "Design process of a triple redundant fault tolerant PMA SynRM," *IEEE Access*, vol. 7, pp. 76241–76249, 2019, doi: 10.1109/ACCESS.2019.2920627.

[12] K.-C. Kim, J. S. Ahn, S. H. Won, J.-P. Hong, and J. Lee, "A study on the optimal design of SynRM for the high torque and power factor," *IEEE Trans. Magn.*, vol. 43, no. 6, pp. 2543–2545, Jun. 2007, doi: 10.1109/TMAG.2007.893302.

[13] L. Ren, G. Lin, Y. Zhao, Z. Liao, and F. Peng, "Adaptive nonsingular finite-time terminal sliding mode control for synchronous reluctance motor," *IEEE Access*, vol. 9, pp. 51283–51293, 2021, doi: 10.1109/ACCESS.2021.3068745.

[14] F.-J. Lin, M.-S. Huang, S.-G. Chen, and C.-W. Hsu, "Intelligent maximum torque per ampere tracking control of synchronous reluctance motor using recurrent Legendre fuzzy neural network," *IEEE Trans. Power Electron.*, vol. 34, no. 12, pp. 12080–12094, Dec. 2019, doi: 10.1109/TPEL.2019.2906664.

[15] T. Pajchrowski, K. Zawirski, and K. Nowopolski, "Neural speed controller trained online by means of modified RPROP algorithm," *IEEE Trans. Ind. Informat.*, vol. 11, no. 2, pp. 560–568, Apr. 2015, doi: 10.1109/TII.2014.2359620.

[16] S. Kouro, P. Cortes, R. Vargas, U. Ammann, and J. Rodriguez, "Model predictive control—A simple and powerful method to control power converters," *IEEE Trans. Ind. Electron.*, vol. 56, no. 6, pp. 1826–1838, Jun. 2009, doi: 10.1109/TIE.2008.2008349.

[17] L. Tarisciotti, P. Zanchetta, A. Watson, J. C. Clare, M. Degano, and S. Bifaretti, "Modulated model predictive control for a three-phase active rectifier," *IEEE Trans. Ind. Appl.*, vol. 51, no. 2, pp. 1610–1620, Mar./Apr. 2015, doi: 10.1109/TIA.2014.2339397.

[18] Y. Zhang and H. Yang, "Two-vector-based model predictive torque control without weighting factors for induction motor drives," *IEEE Trans. Power Electron.*, vol. 31, no. 2, pp. 1381–1390, Feb. 2016, doi: 10.1109/TPEL.2015.2416207.

[19] W. Chen, S. Zeng, G. Zhang, T. Shi, and C. Xia, "A modified double vectors model predictive torque control of permanent magnet synchronous motor," *IEEE Trans. Power Electron.*, vol. 34, no. 11, pp. 11419–11428, Nov. 2019, doi: 10.1109/TPEL.2019.2898901.

[20] W. Song, C. Xue, X. Wu, and B. Yu, "Modulated finite-control-set model predictive current control for five-phase voltage-source inverter," *IEEE Trans. Transport. Electrific.*, vol. 7, no. 2, pp. 718–729, Jun. 2021, doi: 10.1109/TTE.2020.3019208.

[21] H. Li, M. Lin, M. Yin, J. Ai, and W. Le, "Three-vector-based low-complexity model predictive direct power control strategy for PWM rectifier without voltage sensors," *IEEE J. Emerg. Sel. Topics Power Electron.*, vol. 7, no. 1, pp. 240–251, Mar. 2019, doi: 10.1109/JESTPE.2018.2871332.

[22] D. Xu, W. Zhao, H. Tang, X. Song, and R. Xue, "Three-vector-based model predictive current control with zero-sequence current suppression for open-winding LPMVM drives," *IEEE Trans. Veh. Technol.*, vol. 70, no. 1, pp. 225–236, Jan. 2021, doi: 10.1109/TVT.2020.3045257.

[23] L. Tarisciotti, P. Zanchetta, A. Watson, S. Bifaretti, and J. C. Clare, "Modulated model predictive control for a seven-level cascaded H-bridge back-to-back converter," *IEEE Trans. Ind. Electron.*, vol. 61, no. 10, pp. 5375–5383, Oct. 2014, doi: 10.1109/TIE.2014.2300056.

[24] J. Xu, T. B. Soeiro, F. Gao, L. Chen, H. Tang, P. Bauer, and T. Dragicevic, "Carrier-based modulated model predictive control strategy for three-phase two-level VSIs," *IEEE Trans. Energy Convers.*, vol. 36, no. 3, pp. 1673–1687, Sep. 2021, doi: 10.1109/TEC.2021.3073110.

[25] S. S. Yeoh, T. Yang, L. Tarisciotti, C. I. Hill, S. Bozhko, and P. Zanchetta, "Permanent-magnet machine-based starter–generator system with modulated model predictive control," *IEEE Trans. Transport. Electrific.*, vol. 3, no. 4, pp. 878–890, Dec. 2017, doi: 10.1109/TTE.2017.2731626.

[26] C. Xiong, H. Xu, T. Guan, and P. Zhou, "A constant switching frequency multiple-vector-based model predictive current control of five-phase PMSM with nonsinusoidal back EMF," *IEEE Trans. Ind. Electron.*, vol. 67, no. 3, pp. 1695–1707, Mar. 2020, doi: 10.1109/TIE.2019.2907502.

[27] C. A. Agustin, J.-T. Wang, and C.-K. Lin, "A modulated model predictive current controller for four-switch three-phase inverter-fed SynRMs," in *Proc. IEEE 4th Int. Future Energy Electron. Conf. (IFEEC)*, Nov. 2019, pp. 1–5, doi: 10.1109/IFEEC47410.2019.9014991.

[28] C.-K. Lin, T.-H. Liu, J.-T. Yu, L.-C. Fu, and C.-F. Hsiao, "Model-free predictive current control for interior permanent-magnet synchronous motor drives based on current difference detection technique," *IEEE Trans. Ind. Electron.*, vol. 61, no. 2, pp. 667–681, Feb. 2014, doi: 10.1109/TIE.2013.2253065.

[29] C.-K. Lin, J.-T. Yu, Y.-S. Lai, and H.-C. Yu, "Improved model-free predictive current control for synchronous reluctance motor drives," *IEEE Trans. Ind. Electron.*, vol. 63, no. 6, pp. 3942–3953, Jun. 2016, doi: 10.1109/TIE.2016.2527629.

[30] Y. Wang, H. Li, R. Liu, L. Yang, and X. Wang, "Modulated model-free predictive control with minimum switching losses for PMSM drive system," *IEEE Access*, vol. 8, pp. 20942–20953, 2020, doi: 10.1109/ACCESS.2020.2968379.

CHENG-KAI LIN was born in Taipei, Taiwan, in 1980. He received the B.S. degree in electrical engineering from the Ming Chi University of Technology, Taipei, in 2002, and the M.S. and Ph.D. degrees in electrical engineering from the National Taiwan University of Science and Technology, Taipei, in 2004 and 2009, respectively. From October 2009 to August 2012, he was a Postdoctoral Researcher with the Department of Electrical Engineering, National Taiwan University, Taipei. He is currently an Associate Professor of electrical engineering with National Taiwan Ocean University, Keelung, Taiwan. His research interests include motor drive control, power electronic applications, and control applications.

CRESTIAN ALMAZAN AGUSTIN (Graduate Student Member, IEEE) was born in Isabela, Philippines, in 1989. He received the B.S. degree in electrical engineering from Isabela State University, Ilagan, Philippines, in 2012, the M.S. degree in engineering management from the University of La Salette, Santiago, Philippines, in 2015, and the M.S. degree in electrical engineering from the University of St. Louis, Cagayan, Philippines, in 2016. He is currently pursuing the Ph.D. degree in electrical engineering with National Taiwan Ocean University, Keelung, Taiwan. From 2014 to 2017, he was a Resident Engineer at the SM Engineering Design and Development, Pasay, Philippines. In 2018, he joined as a Lecturer with the Electrical Engineering Department, Isabela State University. His research interests include control of motor drives and inverter topologies.

JEN-TE YU was born in Hualien, Taiwan. He received the M.S. degree in aerospace engineering from Wichita State University, USA, the M.S. degree in electrical engineering from the Georgia Institute of Technology, USA, and the Ph.D. degree in electrical engineering from the National Taiwan University, Taiwan.

He has been with the Department of Electrical Engineering, Chung Yuan Christian University (CYCU), Taiwan, as an Assistant Professor, since August 2016, where he currently serves as the Director for the Modern Control Laboratory. Before joining CYCU, he had worked in the industry for years both in the USA and Taiwan as an Engineer and later as a Corporate Research and Development Manager. His current research interests include networked control subject to sporadic packet dropout, linear quadratic regulator theory, consensus of multiagent systems, and output feedback design of negative imaginary systems.

YU-SHAN CHENG (Member, IEEE) received the B.S. and Ph.D. degrees in electrical engineering from the National Taiwan University of Science and Technology, Taiwan, in 2012 and 2017, respectively. From 2015 to 2016, she stayed at the Technical University of Munich, Germany, as a Visiting Scholar. From 2017 to 2020, she worked as a Project Researcher at Tokyo Metropolitan University, Japan. Since 2020, she has been a Faculty Member with the Department of Electrical Engineering, National Taiwan Ocean University. Her current research interests include power management of renewable energy systems, metaheuristic optimization, and power converters.

FU-MIN CHEN was born in Taichung, Taiwan, in 1992. He received the M.S. degree in electrical engineering from the National Taiwan Ocean University, Keelung, Taiwan, in 2016. From 2016 and 2019, he served as an Electrical and Electronic Engineer at Hiwin Mikrosystem Corporation and Nuvoton Technology Corporation. His research interests include predictive control, motor controller design, and integrated circuit design with applications to robotic systems.

YEN-SHIN LAI (Fellow, IEEE) received the M.S. degree in electronic engineering from the National Taiwan University of Science and Technology, Taipei, Taiwan, and the Ph.D. degree in electronic engineering from the University of Bristol, Bristol, England, U.K.

In 1987, he joined the Department of Electrical Engineering, National Taipei University of Technology, Taipei, where he served as the Chairperson, from 2003 to 2006, and has been a Full Professor, since 1999, a Distinguished Professor, since 2006, and a Chair Professor, since 2013. His research interests include control of power converters, inverters, and motor drives.

Dr. Lai received several national and international awards, including the 1995–1996 John Hopkinson Premium from the Institute of Electrical Engineers (IEE), the Technical Committee Prize Paper Award from the IEEE IAS Industrial Drives Committee, in 2002, the Outstanding Paper Award, the International Conference of Renewable Energy Research and Applications, Nagasaki, Japan, in 2012, and the Best Paper Award, IEEE PEDS, Kitakyushu, Japan, in 2013. He received the Outstanding Research Award, Ministry of Science and Technology, Taiwan, in 2013 and 2018. He was also awarded the 2018 Prize Paper Award, IEEE JOURNAL OF EMERGING AND SELECTED TOPICS IN POWER ELECTRONICS, TECO Award, in 2019, and the Award for Industry Collaboration, Ministry of Education, Taiwan, in 2020. He served as the Secretary for IEEE IAS Industrial Drives Committee, from 2008 to 2009, and the Chapter Chair for IEEE IAS Taipei Chapter, from 2009 to 2010. From 2010 to 2013, he served as the Vice Chair for IEEE IAS Industrial Drives Committee, where he was the Chair, from 2014 to 2015. He also served as an Associate Editor for IEEE TRANSACTION ON INDUSTRY APPLICATIONS, from 2008 to 2011, IEEE TRANSACTION ON INDUSTRIAL ELECTRONICS, and *IET Electrical Power Applications*. He also served as the Chair for the Electrical Power Engineering Division, Ministry of Science and Technology, Taiwan, and the President for Taiwan Power Electronics Association, Taiwan, from 2016 to 2019. Since 2011, he has been an elected AdCom member of IEEE Industrial Electronics Society, an Editor of IEEE JOURNAL OF EMERGING AND SELECTED TOPICS IN POWER ELECTRONICS, and the Co-Editor-in-Chief, IEEE TRANSACTION ON INDUSTRIAL ELECTRONICS.